Dynamics of positively charged muonium centers in indium nitride

Y. G. Celebi*
Department of Physics, Istanbul University, 34134 Vezneciler, Istanbul, Turkey

R. L. Lichti and B. E. Coss
Department of Physics, Texas Tech University, Lubbock, Texas 79409-1051, USA

S. F. J. Cox
ISIS Facility, Rutherford Appleton Laboratory, Chilton OX11 0QX, United Kingdom
and Condensed Matter and Materials Physics, University College London, WC1E 6BT, United Kingdom
(Received 24 May 2006; revised manuscript received 2 November 2006; published 29 December 2006)

Muon spin depolarization measurements performed on powdered InN with zero applied magnetic field reveal several positively charged diamagnetic muonium centers. At low temperatures, the Mu^+ ground state is weakly relaxing with the characteristics of local tunneling motion, which changes to thermally activated diffusion above 350 K. Additional signals imply stationary metastable Mu^+ centers, which undergo successive activated transitions into the ground state at temperatures ranging from 250 to 400 K. Above 450 K, the Mu^+ diffusion is interrupted by trap and release events. The high-temperature trapped state is different from any of the low-temperature sites. The energies associated with metastable-to-stable site changes, detrapping transitions, and thermal diffusion are extracted and possible sites for the observed Mu^+ signals are discussed as a model for interstitial protons, H^+.

DOI: 10.1103/PhysRevB.74.245219 PACS number(s): 66.30.Jt, 76.75.+i

I. INTRODUCTION

Hydrogen has the ability to electrically passivate both donor and acceptor impurities, saturate dangling bonds, and to create defect levels of its own. A full understanding of the properties of hydrogen impurities requires determination of the crystallographic sites for isolated H and its diffusion properties in various charge states, as well as characterizing the structure and stability of complexes formed as a result of its reactions with dopants and other defects. Much of the experimental data concerning diffusion and charge-state dynamics of isolated H comes only indirectly from capacitance measurements. However, muonium (Mu), in every practical sense a very light and short-lived radioactive isotope of H, provides us with the means to obtain experimental data from which to extract the dynamics and static properties of the isolated hydrogen impurity.

Mu, as well as H or D, is known to exist in three charge states 0, +1, and −1 in semiconducting media. After implantation of positive muons, a muon may capture an electron to form a neutral muonium atom. Capture of a second electron can occur, especially in *n*-type samples, resulting in a negative (hydride) ion. Chemical notation is adopted to address the muonium charge state, i.e., Mu^+, Mu^0, and Mu^-, with subscripts used to label a specific signal or site. The charge state is an important quantity in determining the interstitial location and relative mobility of muonium impurities. In relatively ionic compounds like the nitrides, Mu^+ will prefer sites closer to a cation, and conversely, Mu^- is attracted to anion related sites.

Aside from studying isolated H through its pseudoisotope, research on muonium is an excellent way to test theoretical models for the sites and barriers to motion of hydrogen. However, special attention is needed to address the differences between hydrogen and muonium. Chemically, muonium behaves essentially the same as hydrogen with analogous atomic states. Due to the mass difference, there could be a change in stable sites and motional dynamics will certainly be modified. Such differences must be taken into consideration when interpreting Mu results for H.

In this paper we address the diamagnetic Mu^+ centers and their motional properties in InN as part of an ongoing program to examine the sites and motion of Mu in the III–V nitrides[1,2] as an experimental model for what can be expected for hydrogen. Previous work[3–5] verified that Mu functions as a shallow donor in InN and that the observed shallow effective-mass Mu^0 center is associated with the most stable location for Mu^+. The present work focuses on the temperature range above Mu^0 ionization, completed by roughly 60 K, where only diamagnetic Mu^+ signals are present.

II. THE BASIC EXPERIMENT

Muon spin relaxation, one of the techniques collectively known as μSR, forms the bulk of our current investigations. Specifically we use the loss of muon spin polarization as a function of time in zero applied magnetic field to probe the muon's interaction with the internal nuclear dipolar fields of InN. All of the μSR methods are based on the results of parity violation in the muon formation and decay processes. Decay of pions yield 100% spin-polarized muons, which are implanted into the sample. The evolution of the muon's spin with time is then monitored through the detection of the emitted positrons. Data collected in a μSR experiment reflect the asymmetry of the muon decay. The spin evolves in the muon's local magnetic environment, thus the decay asymmetry directly probes the muon's interaction with nearby nuclear spins, yielding information on the distribution of lo-

cal dipolar fields as well as any dynamics such as muon motion or transitions that change the muon's immediate environment. In particular, by appropriately grouping opposing detectors, for instance front (F) and back (B), the asymmetry is constructed from the raw data count rates $N_F(t)$ and $N_B(t)$ as

$$a_0 P(t) = \frac{N_F(t) - \alpha N_B(t)}{N_F(t) + \alpha N_B(t)},$$

where a_0 is a constant ($\sim$0.23 to 0.28) and α is a correction factor for small differences in the detector geometries and efficiencies. The parameter α sets the baseline and is determined from spin precession spectra taken in a weak transverse magnetic field with the same sample, detector geometry, and muon beam conditions with which the zero-field data are collected. The value of α is adjusted to center the oscillating precession signal at zero and is then fixed so that zero-field data can be analyzed with any baseline shift effectively removed. The time-dependent asymmetry, or the depolarization function $P(t)$, from analysis of zero-field data allows specific muonium states to be identified and their dynamical properties to be extracted as discussed below.

With zero external magnetic field, the depolarization associated with a stationary diamagnetic muonium state is described by the zero-field static Gaussian Kubo-Toyabe function (s-KT) as

$$Q(t) = \frac{1}{3} + \frac{2}{3}(1 - \Delta_S^2 t^2)\exp\left(-\frac{1}{2}\Delta_S^2 t^2\right). \quad (1)$$

The static rate constant Δ_S is determined by the second moment of the internal magnetic fields at the site where the muon resides. These fields, from magnetic dipoles of the nuclei neighboring the diamagnetic muon center, are assumed to be randomly oriented. For long times, one-third of the initial polarization is recovered. This is simply due to the fact that on average one-third of local field components are parallel to the initial polarization. Observation of a constant 1/3 residual polarization signifies the static nature of the diamagnetic center, and the value of Δ_S provides an identifying label for a particular site.

When a diamagnetic center is moving among equivalent sites with an average hop rate ν, the appropriate form for the depolarization in zero applied field is the dynamic Kubo-Toyabe function (d-KT) given by

$$P_D(t) = Q(t)e^{-\nu t} + \nu \int_0^t d\tau\, Q(\tau) P_D(t-\tau) e^{-\tau\nu}. \quad (2)$$

In order to obtain the proper hop rates when fitting with this function, it is common practice to obtain a good estimate of the static rate constant Δ_S in a temperature region where the center is not mobile, and to fix that parameter in the dynamic regime.

When the maximum range of the time spectrum is short compared to Δ^{-1} or ν/Δ is sufficiently large, the so-called Abragam function,[6] as modified[7] for zero or longitudinal fields,

$$P_A(t) = \exp\left\{-2\frac{\Delta_G^2}{\nu}[\exp(-\nu t) - 1 + \nu t]\right\}, \quad (3)$$

becomes an appropriate approximation to the dynamic Kubo-Toyabe function. In practice, this analytical form was used for weakly relaxing signals from the very mobile Mu^+ ground state in order to allow testing for slow dynamics in other KT signals. If more than one type of site is visited during diffusion, neither Eq. (2) nor Eq. (3) provides a good description of the overall behavior. We discuss such a situation further in the section on high-temperature trap-limited diffusion in InN.

The InN powder sample used for this experiment was purchased from Alfa-Aesar. The zero-field μSR measurements were performed at the EMU beam line of the ISIS facility of Rutherford Appleton Laboratory in England. The initial report[3] on the Mu shallow-donor state in InN was based on data for a different sample from the same source. Identical zero-field signals are observed in the two samples but with different relative amplitudes.

Although at first glance the depolarization curves may suggest only two signals, a detailed analysis indicates that no fewer than four isolated Mu^+ centers are required in order to produce all of the dynamical features seen in these data. In a preliminary report,[5] based on a two-signal analysis of zero-field data on this particular sample, we have shown that the Mu^+ ground state is mobile at all temperatures. Up to 350 K, this center shows the characteristics of local tunneling motion while above 350 K it shows activated long-range thermal motion. An additional faster-relaxing fraction is also observed and has the characteristic Kubo-Toyabe relaxation identifying a static diamagnetic center, which we assign to Mu^+ bound to an N atom at a metastable site or trapped at a defect. The amplitude versus temperature curve for the static fraction in both investigated InN samples[4,5] shows at least two steps in a conversion to the mobile ground state. This implies that there are at least two static Mu^+ states that escape from their metastable locations at different temperatures. The temperature-dependent amplitudes with three components further imply that a fourth state is required in order to properly account for all of the observed features. After assigning a depolarization function to each signal, we used the temperature dependence of amplitudes corresponding to each component to extract transition energies and prefactors. Below, we discuss the procedure for separating the depolarization signal into specific components and for assigning the appropriate static rate constant Δ to each observed Mu^+ center.

III. SIGNAL SEPARATION

Figure 1 displays a sequence of asymmetry data and the corresponding fits with the assigned rate constants for the Mu^+ signals observed in InN. The depolarization data are chosen at four representative temperature points so that different signatures of the observed Mu species can be seen and compared. Visual inspection of the depolarization data clearly indicates that as the temperature is elevated, the overall depolarization rate decreases, implying that Mu^+ becomes

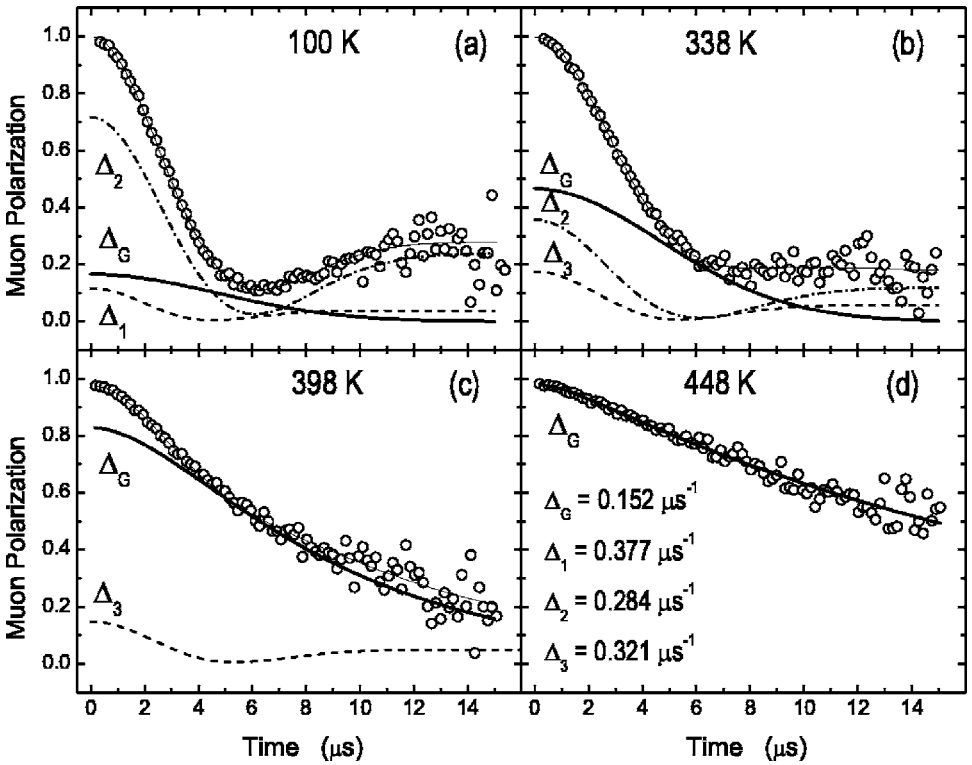

FIG. 1. Fits to zero-field muon spin depolarization data and the component signals for Mu^+ in InN at several temperatures. When the static rate parameters are kept constant, the remaining fit parameters lead to the conversion and motional dynamics discussed in the text.

increasingly more mobile. However, these curves necessitate more than one signal and do not fit to a single-component dynamic function. In pilot fits allowing for multiple dynamic components, we determined that the faster relaxing signal(s) do not show any motion, but that those amplitudes are simply transferred into the ground-state signal. This behavior is to be expected for a simple one-way transition out of a metastable state into the stable one, which happens to be mobile in the present case.

Our primary strategy in separating the depolarization signals into components appropriate to individual Mu^+ sites is that each metastable state should have a single transition into the ground state. The preliminary analysis[5] shows that the main metastable-to-stable site-change transition starts very near 300 K; however, a fairly small fraction begins to undergo a site change closer to 200 K and has a smaller activation energy. The two-state analysis also suggests a second change in slope of the amplitude versus temperature curves roughly halfway through the main site-change transition. In order to produce well defined single transitions out of each state, we were forced to introduce two additional Mu^+ centers, one to account for the 200 K feature and a second to deal with the conversion dynamics above 300 K. Below, we discuss the parameters obtained for each state and the dynamic features present in our final analysis.

From completion of the shallow-donor ionization below 80 K up to 200 K, the depolarization fits extremely well to a sum of two static KT components plus the slowly relaxing signal assigned to the Mu^+ ground state. The three-component fits for 100–200 K yield nearly constant amplitudes and rate parameters: Δ_G for the ground state, and Δ_1 and Δ_2 as the static KT rate parameters for two metastable sites. Thus, we chose to fix these rate constants at their average values in further fits. This yields very smooth amplitude curves and is particularly important at higher temperatures where site-change transitions and the onset of thermally activated ground-state diffusion occur.

The metastable state labels indicate the order in which they disappear with increasing temperature. The amplitude for the static KT component with Δ_2, as shown in Fig. 1(a), stays constant up to nearly 300 K. Between 100 and 300 K, changes in the signal amplitude associated with rate Δ_1 are correlated only with the ground state. Explicitly, as the temperature rises, the Δ_1 signal amplitude decreases while the Δ_G ground-state signal amplitude increases at the same rate. By 300 K, whereas the Δ_2 related amplitude shows no change, the Δ_1 signal has disappeared, converting completely to the ground state. Thus our final analysis shows distinct signals for two low-temperature metastable Mu^+ states with well resolved separate site conversions.

Above approximately 300 K where the signal associated with Δ_1 vanishes, a third static component having a different rate constant Δ_3 appears in conjunction with a decrease in the Δ_2 amplitude. Signal separation in this region is not as clean as below 300 K, and obtaining a good estimate for Δ_3 is somewhat problematic, since it is only present in a region where more than one transition is active. Although the general nature of the results remains the same, parameters obtained for the dynamics of the relevant transitions are strongly coupled with the s-KT rate parameter for this signal. The analysis presented here has Δ_3 fixed roughly in the middle of the range that works well. Figure 1(b) represents the situation between 300 and 360 K where changes in the amplitudes for three signals (Δ_2, Δ_3, and Δ_G) are correlated. This region ends when the amplitude related to the dominant low-temperature metastable state (Δ_2) vanishes.

As an example of the depolarization data between 360 and 450 K, we have chosen the temperature point at 398 K

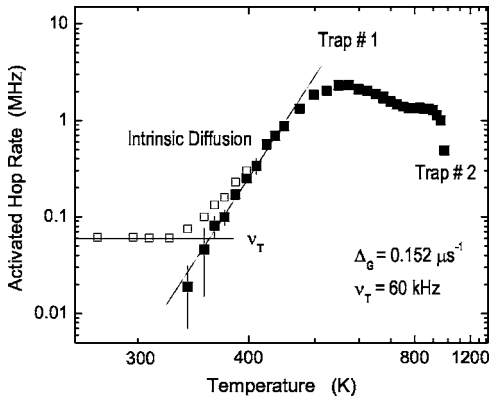

FIG. 2. Zero-field relaxation results for the ground state Mu^+ center in InN. Hop rates obtained with Δ_G fixed imply local tunneling below 350 K (open squares are the total hop rate) and activated diffusion (filled squares) at higher temperatures. Deviations from Arrhenius behavior above 450 K suggest trapping of the mobile Mu^+.

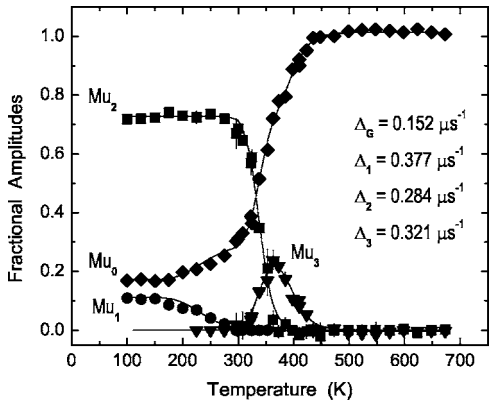

FIG. 3. Amplitudes from zero-field depolarization results for InN showing transitions to the mobile Mu^+ ground state. Fits to these data yield the site-change parameters in Table I.

shown in Fig. 1(c). In this range, we have a two-signal fit with straightforward correlations. The amplitude for the static KT signal with rate Δ_3 decreases as the temperature is elevated, while the amplitude for the ground state continues to increase but at a slower rate, reaching a constant value above 450 K where it represents all the muons.

Figure 1(d) sets an example where a single dynamic function with a constant amplitude describes the zero-field data. In this region, all the muons are diffusively mobile up to about 500 K, at which point the average hop rate starts to decrease, implying trap and release events as discussed in the next section.

Figure 2 displays the hop rates obtained for the Mu^+ ground state from the analysis discussed above in which the static width parameter Δ for each state was fixed at its average free-fit value. With $\Delta_G=0.152\ \mu s^{-1}$, these results imply tunneling motion with a constant rate ν_T of about 60 kHz up to 350 K. Because Δ_G is quite low compared to what is expected for a static Mu^+ bound to nitrogen, as is expected[8,9] for any of the III–V nitrides, this motion is assigned to localized tunneling among different bond orientations around a single N atom. Very similar overall results can be obtained with a larger value for Δ_G and a corresponding increase in the tunneling rate. The upper range of values that do not introduce significant modifications to the motion or transition dynamics at higher temperatures are roughly $\Delta_G=0.240\ \mu s^{-1}$ and $\nu_T=200$ kHz. We conclude that the local tunneling rate for the Mu^+ ground state in InN is considerably less than 0.3 MHz, much slower than the 2–5 MHz tunneling rates seen in AlN and GaN. This uncertainty in Δ_G and ν_T is a consequence of not having access to a region where the Mu^+ ground state is truly static.

The increase in hop rates starting near 350 K represents thermally activated motion, which we interpret as hops from one nitrogen to another and thus a switch to long-range diffusion of Mu^+. As reported earlier,[4] the activation barrier for motion determined from an Arrhenius plot is about 420 meV with a prefactor of $\sim 10^5$ MHz. Figure 2 suggests that further analysis is required for better understanding of the high-temperature behavior of Mu^+ in InN. The diffusion starts to deviate from its intrinsic character at about 480 K as evidenced by the deviation of the hop rates from Arrhenius behavior. This suggests that trapping events are interrupting the long-range motion at a significant rate. As the temperature increases, the average muon hop rate reaches a maximum at about 570 K, then decreases at higher temperatures becoming almost constant between 750 and 900 K, suggesting a balance between trap and release rates and the instantaneous diffusing fraction. Above 900 K, Mu^+ may encounter a different trap as evidenced by a further reduction of the hop rate.

Before discussing our approach to the high-temperature diffusion and trapping dynamics, we return briefly to the low-temperature metastable Mu^+ states. Figure 3 represents our current best attempt to separate the four Mu^+ signals present below roughly 450 K. Following the initial signal separation, we performed a final series of checks that the static rate parameters remained self-consistent. Noting that near 300 K there are only two signals present, a two-state fit consisting of one dynamic and one static function with all parameters free yielded depolarization rate constants of $\Delta_2=0.284\ \mu s^{-1}$ for the static signal and $\Delta_G=0.152\ \mu s^{-1}$ for the slowly relaxing ground state, both extremely close to previous values. Then in order to confirm the static dipolar parameters for the two remaining Mu^+ centers, these values were fixed and three-signal fits below and above this temperature yielded average values of $\Delta_1=0.377\ \mu s^{-1}$ for the additional center at low temperatures and $\Delta_3=0.321\ \mu s^{-1}$ for the one at higher temperatures. Both are only slightly shifted from the initially extracted values.

The final set of amplitudes (Fig. 3) and ground-state hop rates (Fig. 2) are from fits with all four of the static dipolar Δ's fixed at the values presented above and in Table I. Our overall estimates for the accuracy of these static KT rate constants are roughly 1% for Mu_2^+, and perhaps 3% and 5% at best, for Mu_1^+ and Mu_3^+, respectively. For the ground state, Mu_0^+, the combined effect of Δ_G and the low-temperature local tunneling rate ν_T is better than 1%, but as discussed earlier, because of the very strong coupling between these two parameters, their individual values are quite poorly determined. However, the net effect is that the depo-

TABLE I. Parameters for the zero-field depolarization signals assigned to diamagnetic Mu^+ centers in InN, and the energies and prefactors obtained for ground-state motion and transitions out of the tentatively assigned metastable locations.

Muonium state	Site assignment	Static rate constant (μs^{-1})	Transition assignment	Barrier (meV)	Prefactor (MHz)
Mu_0^+	$AB_\perp$	$\Delta_G=0.152$	GS diffusion	421	8.2×10^4
Mu_1^+	$AB_\parallel$	$\Delta_1=0.377$	$Mu_1^+\rightarrow Mu_0^+$	219	4.7×10^{-2}
Mu_2^+	$BC_\parallel$	$\Delta_2=0.284$	$Mu_2^+\rightarrow Mu_3^+ + Mu_0^+$	877	1.2×10^7
Mu_3^+	$BC_\perp$	$\Delta_3=0.321$	$Mu_3^+\rightarrow Mu_0^+$	880	1.5×10^5

larization associated with Mu_0^+ is very accurately represented up to roughly 500 K where trapping at some other defect becomes important.

Finally, to obtain the energy barriers related to transitions out of the three metastable Mu^+ sites, we performed sigmoidal fits to the temperature-dependent amplitudes shown in Fig. 3 with appropriately shared parameters. These data result in the following sequence of transfers from one site to another as the temperature is raised. First, Mu_1^+ overcomes a barrier of about 220 meV to join the locally mobile ground state in a transition centered near 250 K. Second, starting at about 280 K, Mu_2^+ transforms into the species labeled as Mu_3^+, presumably as a site-change transition, with some fraction going directly to the ground state. The final site-change transition occurs near 400 K when the intermediate state Mu_3^+ converts to the ground state, which is diffusively mobile by that temperature. The barriers for exit from the sites associated with Mu_2^+ and Mu_3^+ are essentially identical but the prefactors differ by two orders of magnitude. This qualitative result was consistent for any set of Δ's we tried. Based on the energy variations for the different sets, we estimate that the barriers for Mu_0^+ motion and exit from the metastable site for Mu_1^+ have an uncertainty of $\sim$5% while the larger barrier(s) for Mu_2^+ and Mu_3^+ have 15–20% uncertainty.

It should be emphasized here that what we are discussing as site-change transitions extracted from the amplitude conversions are in some sense just the final step in thermalization of implanted muons. At lower temperatures, the muons lose sufficient energy entering the metastable site that they remain trapped there on the μSR time scale, while at higher temperatures the lattice vibrational energy is sufficient to help them escape from that site quickly. The barriers we obtained should be reasonably accurate in representing the energy landscape into which the muons are being implanted. What we do not obtain from this analysis because of the nonequilibrium site populations is any indication of the relative energies for minima associated with the metastable sites. Our final set of barrier energies and prefactors is listed in Table I along with state identifications, the static dipolar rate constants, and transition assignments. Arguments pertaining to Mu^+ site assignments are presented in a later section, but we include those results in Table I for convenience.

IV. HIGH-TEMPERATURE TRAPS

As discussed in the previous section, when the depolarization data are treated with a single dynamic function with Δ_G fixed to represent the diffusing Mu^+ ground state, the extracted hop rates deviate from simple thermally activated behavior above 500 K. These fits indicate that the high-temperature motion is significantly slower than expected from an Arrhenius law, implying that diffusion is interrupted by trapping.

One possibility for such interruptions is that the rapidly diffusing Mu^+ encounters a completely different low-density trap, in which case the trap and release dynamics are unlikely to show any correlations with known site parameters, and the encounter rate will be limited by diffusion of the free Mu^+. For this situation, there may or may not be a local barrier that needs to be overcome to enter the trap site once it is encountered. In nearly all cases in which an extrinsic defect-related muonium center has been confirmed, one or more of the intrinsic Mu centers show features characteristics of rapid diffusion under the same conditions.

Coupled equations governing the muon depolarization resulting from trap and release dynamics are easily established within a two-state model.[8,10,11] In integral form, these equations are

$$P_T(t) = e^{-\nu_r t}Q_T(t) + \nu_r\int_0^t d\tau\, Q_T(t-\tau)P_F(\tau)e^{-(t-\tau)\nu_r},$$

$$P_F(t) = e^{-\nu_c t}P_A(t) + \nu_c\int_0^t d\tau\, P_A(t-\tau)P_T(\tau)e^{-(t-\tau)\nu_c},$$

where the freely diffusing and trapped states are represented by the subscripts F and T, respectively, and ν_c (ν_r) are the Mu^+ capture (release) rates. We have used $P_A(t)$ as defined in Eq. (3) to describe the evolution of muon polarization while in the diffusing state using previously defined parameters from Table I. The polarization while in the trapped state is described by $Q_T(t)$, which is properly a static KT function with Δ_T as a fit parameter.

Under nonequilibrium conditions, an expansion with terms representing the first few trap or release events can be constructed as

$$P(t) = A_F[e^{-\nu_c t}P_A(t) + \nu_c e^{-\nu_r t}f(t)] + A_T[e^{-\nu_r t}Q_T(t) + \nu_r e^{-\nu_r t}f(t)] + \nu_c\nu_r\int_0^t d\tau\, e^{-\nu_r(t-\tau)}f(t-\tau)[P_A(\tau) + Q_T(\tau)], \quad (4)$$

where $f(t)$ is given by

$$f(t) = \int_0^t d\tau\, Q_T(t-\tau) P_A(\tau) e^{-(\nu_c - \nu_r)\tau}.$$

In pilot fits, the last term in Eq. (4) made a negligible difference in the results, thus it was not included in the final analysis since it greatly increases the computational effort required.

In order to quantitatively model the high-temperature trap and release dynamics for Mu^+ in our powdered InN sample, we made the following approximations based on initial fits with all parameters free. First, use of the two-state treatment implies assumption of a single type of trap site. Second, Mu^+ capture at that trap is assumed to be a simple diffusion-limited process. Since the diffusion is directly related to the known muon hop rate $\nu = \nu_0 \exp(-E_a/kT)$, we treated the capture rate as $\nu_c = \nu_{c0} \exp(-E_a/kT)$. These fits then require ν_r, ν_{c0}, and Δ_T as parameters, along with A_F and A_T representing the initial fractions in the two states. Since ν_{c0} was treated as a free parameter in fits to depolarization curves at each temperature, any local barrier to Mu^+ capture will yield activated behavior for that prefactor.

In order to test whether this two-state model yields results consistent with those of the previous section, we treated the 370–500 K region with the trap and release model. In this temperature range, the only states present in Fig. 3 are the slowly diffusing Mu_0^+ and metastable Mu_3^+. The trap and release fits with all parameters free gave results fully consistent with the earlier treatment. If we set $\Delta_T = \Delta_3 = 0.321\ \mu s^{-1}$ and fix the barrier for release to $E_r = 880$ meV as obtained previously for Mu_3^+, the two-state model gives a capture prefactor of $\nu_{c0} \simeq 290$ MHz and a release rate prefactor of $\nu_{r0} = 1.0 \times 10^{10}$ MHz. The (free) converting amplitudes yield parameters very close to those in Table I, which were obtained from the metastable site approach. As expected, these results yield extremely slow capture rates at metastable site 3: a more correct model in this regime would include a large local barrier to this capture process, resulting in even smaller trapping rates.

To further quantify the dynamics in this temperature region, the two-state results imply about 266 jumps for the diffusing Mu^+ before it would trap at site 3. Compared to its 2.2 μs mean lifetime, at 398 K the muon spends an average of 2.7 μs at each site along its diffusion path and would be captured after about 720 μs. Additionally, at this temperature, a muon trapped as Mu_3^+ spends approximately 13 μs at the metastable site before it is released. By about 450 K this average residence time as Mu_3^+ has decreased to less than 1 μs, consistent with this state not being seen above 480 K in Fig. 3.

When all of the parameters are left free in the two-state trap and release model, there is an abrupt change in Δ_T from a value consistent with Mu_3^+ below 450 K to less than 0.040 μs^{-1} above 500 K, and the A_T corresponding to Mu_3^+ drops to zero by 500 K as well. Over the range of 500–700 K, the average value for Δ_T is 0.022 μs^{-1}, implying that the active trap site does not contain a close neighbor with any significant magnetic moment, electronic or nuclear, effectively ruling out a site intrinsic to bulk InN. In this region, the trapping rate ν_c far exceeds the release rate ν_r and one can get good fits by assuming zero probability for release.

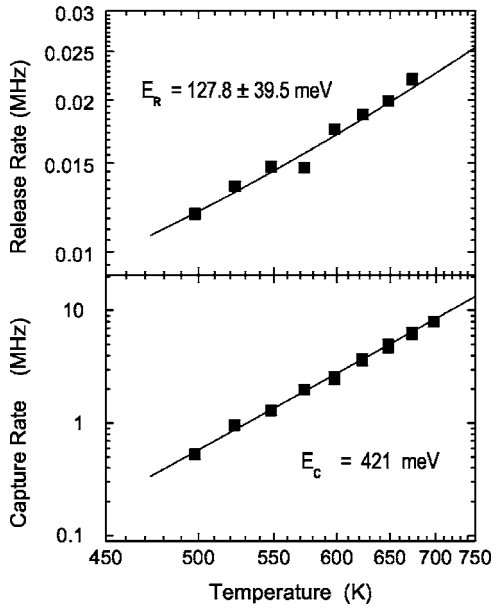

FIG. 4. Capture and release rates for Mu^+ at the high-temperature trap characterized by $\Delta_T = 0.022\ \mu s^{-1}$. Arrhenius fits to these results yield the parameters in Table II.

Figure 4 and Table II show the Mu^+ capture and release results obtained with all parameters free. The release rates show an activated behavior; however, both the energy parameter $E_r = 128 \pm 40$ meV and prefactor $\nu_{r0} = 150 \pm 70$ kHz are extremely low compared to those obtained for escape from any of the metastable locations seen at lower temperatures. In addition, the initially trapped fraction increases rapidly above 600 K, and by 700 K the initially free fraction is observed directly as a small-amplitude fast-relaxing component. Although the fits became increasingly unstable above 700 K, a continuation of these relationships reproduces the data quite well up to near 850 K. As stated earlier, there is evidence for a second trap that becomes active above 900 K; however, there are too few points to get much information except that this trap appears to produce a much larger Δ_T and requires a local barrier to enter the trap site, more consistent with a low-temperature metastable site except that it is much more strongly bound.

Again looking at how the various characteristic times compare to the muon lifetime, we find a large degree of internal consistency. For example, at 523 K the muon spends an average of 0.14 μs at each site along its diffusion path

TABLE II. Parameters for Mu^+ capture and release rates extracted using the two-state model, including the mean number of jumps $N = \nu_0/\nu_{c0}$ before capture.

Range (K)	Δ_T (μs^{-1})	ν_{c0} (MHz)	ν_{r0} (MHz)	E_r (meV)	N
370–470	0.321	290	1.0×10^{10}	880	266
500–700	0.022	8640	1.5×10^{-1}	128	10

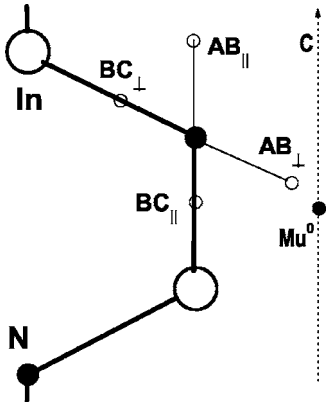

FIG. 5. Possible diamagnetic Mu^+ sites coplanar with the In-N bond chain. The expected site for the (unstable) Mu^0 trapped atom is shown on the channel axis near $AB_\perp$ assigned to the Mu^+ ground state. Out-of-plane atoms are not shown.

and is captured after 1.33 μs, yielding only about 10 jumps to reach the high-temperature trap. At this temperature the muon remains trapped for an average of 110 μs before it is released. By 673 K, the mean total time in the diffusing state has decreased to 0.18 μs while the time in the trapped state is still 59 μs, extremely long compared to the 2.2 μs lifetime. The short mean capture time above 650 K is consistent with a large fraction of implanted muons appearing to be initially trapped and a small free initial fraction showing the Mu^+ trapping rate as a fast exponential transient, typical of the qualitative features observed in the raw data.

V. POSSIBLE SITES FOR MUONIUM

A discussion of likely crystallographic sites for the various muonium species is made more complete by addressing the III-nitride compounds as a group. GaN, AlN, and InN are all stable in the 2*H* wurtzite crystal structure and have significant ionic character to the III-N bonds, InN being the most ionic of this group. It is reasonable to expect the properties of hydrogen to be similar in all three of these compounds. Because of the ionic character of the host bonds, H or Mu in the positive charge state will be attracted to the N atoms, while the negative ionic state of H or Mu will be attracted to the group-III atom, indium in the present case. The Mu^0 hyperfine constants extracted from decoupling curves[2,12] are close to the free Mu^0 value for GaN and AlN, characteristic of a simple trapped atom. For InN, it appears that atomic H or Mu is unstable against complete delocalization of the unpaired electron into the conduction band: the only neutral Mu state observed is the shallow donor, which has the Mu^+ ground state as its core, as we have previously demonstrated.[5] Models[9,13] that predict shallow donor behavior for H in InN also imply that the negatively charged ionic state will be unstable.

Various theoretical results[9,13,14] for GaN find a series of Mu^+ sites near the nitrogen atom. Figure 5 shows nitrogen-related sites for Mu^+ that are coplanar with the In-N bond chain in InN. There are a total of eight predicted Mu^+ sites associated with each N atom. Four are bond-centered locations, three of which are equivalent with N-Mu^+ oriented at roughly 70° to the *c* axis ($BC_\perp$), and the fourth has N-Mu^+ parallel to the symmetry axis ($BC_\parallel$). There are also four possible sites at the so-called antibonding locations; three ($AB_\perp$) with N-Mu^+ oriented into the channel regions of the structure directly opposite the bonds, and one located within the blocked cagelike region ($AB_\parallel$).

The data discussed in the previous section imply a mobile Mu^+ ground state and are consistent with observed Mu^+ signals in both AlN and GaN.[2,15–17] The $AB_\parallel$ site has the highest energy, but the ordering of the other three sites seems to depend on details of the calculational method.[14] In GaN, we observed[2] a mobile Mu^+ ground state plus a single stationary excited state assigned to the $AB_\parallel$ site. We have argued that the zero-point energy for Mu^+ is likely larger than the barriers between the three lower energy locations, leading to a single mobile state characterized by low-temperature tunneling rates on the order of 5 MHz.[2] The observation of four separate Mu^+ signals and much slower tunneling rates in InN suggests larger barriers between the various Mu^+ sites than for AlN or GaN, allowing for four distinct types of N-related locations. We argue that the tunneling ground state in all of these nitrides is most likely for the three $AB_\perp$ sites surrounding a single N atom to which it is strongly bound, since that ought to require less lattice rearrangement than would be required to set up a tunneling state involving the three $BC_\perp$ sites.

Having assigned the $Mu_0{}^+$ state to the nitrogen $AB_\perp$ sites, we turn to the other diamagnetic centers observed in InN. Site determination for stationary Mu^+ or Mu^- centers can be accomplished via a form of level crossing resonance (LCR). Briefly, in this method a magnetic field applied parallel to the initial muon spin direction tunes the Zeeman splitting for the muon into resonance with the quadrupole splitting for the neighboring nucleus. Resonant cross relaxation then takes place reducing the muon spin polarization, which is observed as a resonance line. The strengths and location of these resonances are directly proportional to the muon-nucleus dipole-dipole and muon-induced quadrupole interactions, respectively, thus they are signatures of the local muon site. The resonant polarization transfer is very sensitive to muon motion, and at the onset of diffusion or a site-change transition the associated LCR spectrum weakens and broadens, disappearing for a rapidly diffusing center.

Level-crossing spectra obtained at several temperatures for both InN samples are quite noisy due to relatively low statistics. The observed signals are powder averaged, making it difficult to accurately define the local structure of the observed state, nevertheless we can gain some useful information. Figure 6 displays the LCR data at two temperatures, showing a single peak that identifies the neighbor as nitrogen. This line broadens and weakens as the temperature increases in a manner that is strongly correlated with the zero-field signal for the $Mu_2{}^+$ state as shown in Fig. 3. This LCR peak shows a shift toward lower field with increasing temperature as it broadens. The reason for this shift is not yet well understood, but it is very similar to the behavior seen for the metastable Mu^+ state in GaN, which was assigned to the $AB_\parallel$ site.

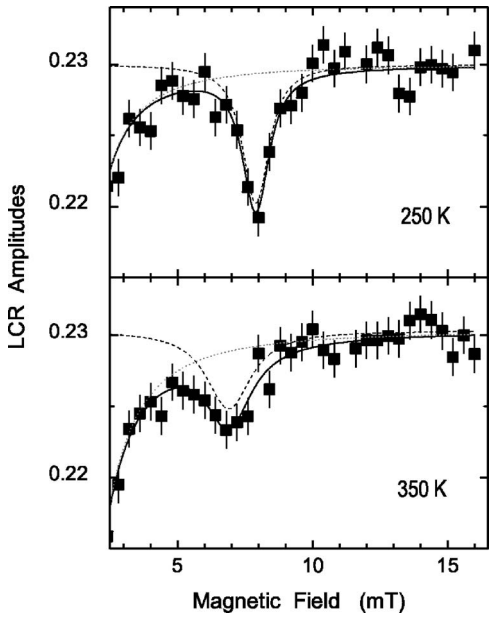

FIG. 6. Level crossing resonances for a metastable Mu^+ center at two temperatures. The broadening at higher temperature implies a transition out of that state which correlates well with that of Mu_2^+ in Fig. 3.

It should be possible to assign the four observed Mu^+ signals in InN to the four N-related sites, intrinsic to the wurtzite structure, based on the local fields expected at the different locations. The KT static Δ values from Table I measure these local nuclear dipolar fields. We have already discussed the range of Δ_G and tunneling rates consistent with the ground-state Mu^+ signal. These values and our assignment of $AB_\perp$ as the basic ground-state location are consistent with the fact that this site should have the smallest mean local field of the four. Although details of the lattice relaxation associated with each site are required in order to accurately model these dipolar fields, BC sites will generally have larger local fields than AB locations. Thus, the two BC sites may be associated with the signals Mu_1^+ and Mu_3^+, and the second antibonding location $AB_\parallel$ is most appropriate for Mu_2^+ based on this argument. This last assignment is fully consistent with conclusions drawn from the level-crossing data as just discussed.

Mu_1^+ shows conversion to the ground state at the lowest temperature, implying that it is the least stable of the metastable locations. The conversion energy of about 0.2 eV would appear appropriate for a simple rotation of the N-Mu^+ bond from $BC_\parallel$ to an adjacent $AB_\perp$ orientation, requiring a minimum of lattice restructuring. We can therefore make a preliminary assignment of Mu_1^+ to $BC_\parallel$, pending arguments regarding Mu_3^+.

As the temperature increases, the Mu_2^+ center assigned to $AB_\parallel$ partially converts to the mobile ground state Mu_0^+, but a significant fraction also populates Mu_3^+. The $AB_\parallel$ assignment for Mu_2^+ means that it resides within the cage part of the InN wurtzite structure. One can reasonably assume that the saddle point for exit from this cage is likely to be midway between two of the three 70° bonds involving the N atom to which it is bound. From this saddle point, continued rotation in the same plane leads to the ground-state $AB_\perp$ site while there are $BC_\perp$ sites to either side. This exit route argument is consistent with an assignment of Mu_3^+ to the $BC_\perp$ locations. A simple branching ratio for the exit from Mu_2^+ would appear to favor Mu_3^+ over Mu_0^+; however, if our arguments are correct, the extra lattice relaxation requirements for entry into the $BC_\perp$ sites should make that path less probable. The experimental branching ratio in the analysis of Fig. 3 is roughly 60/40 in favor of the ground state.

The Mu_3^+ appears to be the most stable of the metastable centers. It is populated above room temperature by conversion from Mu_2^+ and depopulated above 450 K requiring approximately the same energy as the exit from Mu_2^+ but with a much smaller prefactor. However, the arguments we have put forward for a low-energy path out of $BC_\parallel$ to $AB_\perp$ should also apply for the $BC_\perp$ to $AB_\perp$ transition. It may be that our technique of separating the zero-field depolarization data into simple static and dynamic functions somewhat artificially separated the single-step and two-step exit routes from Mu_2^+, and in fact the high barrier and low prefactor assigned to the final step may actually reflect the full dynamics of $AB_\parallel$ to $BC_\perp$ to $AB_\perp$.

Within a simple classical model taking into account the mass difference, the results we have obtained for various Mu centers in InN are qualitatively applicable to the analogous H impurities. The most important factor due to the large mass ratio is the vibrational zero-point energy, which is enhanced by a factor of 3 for Mu centers. This increased zero-point energy of the Mu impurities effectively reduces the energy barrier for exit from the predicted sites. The barriers for thermal motion or for site-change transitions out of metastable locations for H impurities are expected to be higher by several tenths of an eV. Theoretical work on GaN,[14,18] for instance, claims from 0.2 to 0.5 eV in differences between the zero-point energies of the two pseudo-isotopes. Thus, an upper limit around 0.9 eV should be expected for the classical diffusion barrier for positive hydrogen ions in InN with respect to the 0.4 eV we claim for the corresponding Mu center. In some cases, this barrier may also be modified due to the different lattice relaxations for different masses. Furthermore, the de Broglie wavelength corresponding to Mu^+ is about twice as large as the one for H^+. Quantum-mechanical tunneling effects would be expected to be much more probable for the much lighter Mu species compared to H impurities. Therefore the tunneling rate we observe for the ground state might be far less apparent for hydrogen. Translating the present results for various Mu^+ centers to describe the respective H centers requires a much more detailed model that takes into account possible differences in the potential energy surfaces on which Mu^+ and H^+ move.

VI. CONCLUSIONS

We have identified four distinct Mu^+ states in InN. Three of these centers are characterized by static KT zero-field depolarization signals with fairly large rate constants, while the final one has a small relaxation rate typical of motional dynamics. Based on amplitude conversions, the weakly relaxing signal is associated with the Mu^+ ground state in InN.

Motional properties of the ground state Mu^+ are characteristic of quantum-mechanical tunneling below 300 K, with an estimated tunneling rate of roughly 100 kHz, which we interpret as local motion around a single N atom. At higher temperatures, the motion shows increased hop rates that we interpret as long-range thermal diffusion. The onset of activated motion yields a barrier of around 420 meV. At temperatures above roughly 500 K, the Mu^+ motion exhibits diffusion-limited trapping and slow release dynamics. Based on theoretical results and similarity with mobile Mu^+ states in GaN and AlN, we have assigned the Mu^+ ground state in InN to the nitrogen $AB_\perp$ sites with N-Mu^+ oriented into the channels of the 2*H* wurtzite structure.

Observation of four distinct Mu^+ signals in InN would be consistent with large barriers between the four sites predicted for H^+ in the 2*H* wurtzite structure, as opposed to the small energy differences found by theory and consistent with muonium results in GaN and AlN. We present a possible assignment scheme involving the four predicted minima for N-Mu^+ bond orientations based on the observed depolarization rates and amplitude conversions. We have extracted the site-change barriers for transitions among the four Mu^+ centers observed below 450 K.

The assignment of these states to the four predicted N-Mu^+ bond orientations appears to be feasible. A diamagnetic state seen at low temperatures could be a defect-related Mu center formed during thermalization; however, the large local barrier that is apparently present for entry into each of these sites seems to be more appropriate for isolated metastable Mu^+ states. Clearly, although not likely to be available in the near future, single-crystal samples would prove extremely helpful in verifying that the observed states are isolated Mu^+ centers and for checking detailed site assignments and local restructuring of the host lattice.

Two additional defect-related trap sites are inferred from the behavior of the Mu^+ diffusion dynamics at high temperatures. By using depolarization functions appropriate for a two-state trap and release model, we have determined the Mu^+ capture and release rates together with the associated barriers for one of these trap sites. A very low static depolarization rate indicates that this trap has no magnetic moments in the immediate neighborhood, suggesting sites in vacancies, dislocations, grain boundaries, or other voids. Features associated with an additional trap site appear only at the highest temperatures. This second high-temperature Mu^+ trap appears to present a large local barrier for the mobile Mu^+ to form this strongly bound state.

ACKNOWLEDGMENTS

This work was supported by the U.S. National Science Foundation, the Welch Foundation, and by the Royal Society of London, UK.

*Electronic address: gcelebi@istanbul.edu.tr

[1] R. L. Lichti, Y. G. Celebi, S. P. Cottrell, S. F. J. Cox, and E. A. Davis, J. Phys.: Condens. Matter **87**, S4721 (2004).
[2] R. L. Lichti, Physica B **326**, 139 (2003).
[3] E. A. Davis, S. F. J. Cox, R. L. Lichti, and C. G. V. de Walle, Appl. Phys. Lett. **82**, 592 (2003).
[4] Y. G. Celebi, S. F. J. Cox, E. A. Davis, and R. L. Lichti, Physica B **340**, 385 (2004).
[5] R. L. Lichti, Y. G. Celebi, S. F. J. Cox, and E. A. Davis, J. Phys.: Condens. Matter **16**, 325 (2004).
[6] A. Abragam, *Nuclear Magnetizm* (Oxford University Press, Oxford, 1961).
[7] A. Keren, Phys. Rev. B **50**, 10039 (1994).
[8] D. Richter and T. Springer, Phys. Rev. B **18**, 126 (1978).
[9] J. Neugebauer and C. G. Van de Walle, Phys. Rev. Lett. **75**, 4452 (1995).
[10] C. Boekema, R. H. Heffner, R. L. Hutson, M. Leon, M. E. Schillaci, W. J. Kossler, M. Numan, and S. A. Dodds, Phys. Rev. B **26**, 2341 (1982).
[11] K. W. Kehr, G. Honig, and D. Richter, Z. Phys. B **32**, 49 (1978).
[12] H. N. Bani-Salameh, Y. G. Celebi, S. F. J. Cox, and R. L. Lichti, Physica B **374–375**, 372 (2006).
[13] S. Limpijummong and C. G. V. de Walle, Phys. Status Solidi B **228**, 303 (2001).
[14] A. F. Wright, C. H. Seager, S. M. Myers, D. D. Koleske, and A. A. Allerman, J. Appl. Phys. **94**, 2311 (2003).
[15] M. R. Dawdy, R. L. Lichti, S. F. J. Cox, T. L. Head, B. Hitti, and C. Schwab, Physica B **289**, 542 (2000).
[16] R. L. Lichti, S. F. J. Cox, M. R. Dowdy, T. L. Head, B. Hitti, R. J. Molnar, C. Schwab, and R. P. Vaudo, Physica B **289**, 542 (2000).
[17] R. L. Lichti, Y. G. Celebi, K. H. Chow, B. Hitti, and S. F. J. Cox, Physica B **340**, 430 (2003).
[18] S. K. Estreicher and M. Sanati, Physica B **374–375**, 363 (2006).